

See discussions, stats, and author profiles for this publication at: <https://www.researchgate.net/publication/26775174>

Chemical Synthesis of Two Series of Nerve Agent Model Compounds and Their Stereoselective Interaction with Human Acetylcholinesterase and Human Butyrylcholinesterase

ARTICLE *in* CHEMICAL RESEARCH IN TOXICOLOGY · SEPTEMBER 2009

Impact Factor: 3.53 · DOI: 10.1021/tx900096j · Source: PubMed

CITATIONS

22

READS

30

10 AUTHORS, INCLUDING:



Mary Macdonald

Johnson & Johnson

15 PUBLICATIONS 180 CITATIONS

SEE PROFILE



Shubham Vyas

Colorado School of Mines

40 PUBLICATIONS 434 CITATIONS

SEE PROFILE

Published in final edited form as:

Chem Res Toxicol. 2009 October ; 22(10): 1669–1679. doi:10.1021/tx900096j.

Chemical synthesis of two series of nerve agent model compounds and their stereoselective interaction with human acetylcholinesterase and human butyrylcholinesterase

Nora H. Barakat^{*,†}, Xueying Zheng^{*,†}, Cynthia B. Gilley[†], Mary MacDonald[†], Karl Okolotowicz[†], John R. Cashman[†], Shubham Vyas[‡], Jeremy M. Beck[‡], Christopher M. Hadad[‡], and Jun Zhang^{#,†}

[†]Human BioMolecular Research Institute, 5310 Eastgate Mall, San Diego, CA 92121

[‡]Department of Chemistry, The Ohio State University, 100 West 18th Avenue, Columbus, OH 43210

Abstract

Both G- and V-type nerve agents possess a center of chirality about phosphorus. The S_p -enantiomers are generally more potent inhibitors than their R_p -counterparts toward acetylcholinesterase (AChE) and butyrylcholinesterase (BChE). To develop model compounds with defined centers of chirality that mimic the target nerve agent structures, we synthesized both the S_p and R_p stereoisomers of two series of G-type nerve agent model compounds in enantiomerically enriched form. The two series of model compounds contained identical substituents on the phosphorus as the G-type agents, except that thiomethyl ($\text{CH}_3\text{-S-}$) and thiocholine ($(\text{CH}_3)_3\text{NCH}_2\text{CH}_2\text{-S-}$) groups were used to replace the traditional nerve agent leaving groups (i.e., fluoro for GB, GF, and GD; and cyano for GA). Inhibition kinetic studies of the thiomethyl- and thiocholine-substituted series of nerve agent model compounds revealed that the S_p enantiomers of both series of compounds showed greater inhibition potency toward AChE and BChE. The level of stereoselectivity, as indicated by the ratio of the bimolecular inhibition rate constants between S_p and R_p enantiomers, was greatest for the GF model compounds in both series. The thiocholine analogs were much more potent than the corresponding thiomethyl analogs. With the exception of the GA model compounds, both series showed greater potency against AChE than BChE. The stereoselectivity (i.e., $S_p > R_p$), enzyme selectivity, and dynamic range of inhibition potency contributed from these two series of compounds suggest that the combined application of these model compounds will provide useful research tools for understanding interactions of nerve agents with cholinesterase and other enzymes involved in nerve agent and organophosphate pharmacology. The potential of and limitations for using these model compounds in the development of biological therapeutics against nerve agent toxicity are also discussed.

Keywords

Organophosphorus compounds; nerve agent model compounds; acetylcholinesterase; butyrylcholinesterase; phosphorylation; kinetics

norabarakat@hotmail.com xzheng@hbri.org cgilley@hbri.org mmacdonald@hbri.org kokolotowicz@hbri.org jcashman@hbri.org svyas@chemistry.ohio-state.edu jbeck@chemistry.ohio-state.edu hadad@chemistry.ohio-state.edu jzhang@hbri.org. #Corresponding author: Jun Zhang Human BioMolecular Research Institute 5310 Eastgate Mall, San Diego, CA 92121 Tel: 858-458-9305 Fax: 858-458-9311 jzhang@hbri.org.

*Equal contribution from NB and XZ

Introduction

Nerve agents are a subfamily of organophosphorus compounds (OPs) developed for chemical warfare. Their central nervous system toxicity is caused by irreversible inhibition of acetylcholinesterase (AChE) (1). The inhibition of both AChE and the serum cholinesterase, butyrylcholinesterase (BChE), by OPs occurs through nucleophilic attack of the active site serine on the phosphorus atom. The active site serine residues for both AChE and BChE are located at the bottom of a deep gorge (2,3). Phosphonate binding into this site is controlled by four factors: 1) the oxyanion hole, that interacts strongly with the phosphoryl oxygen; 2) the pi-cation binding site, that is designed to interact with the choline moiety of the normal substrate; 3) the acyl binding site, that is on the opposite side of the active site from the pi-cation binding site; and 4) the gorge. Due to the restricted availability of authentic nerve agents, OPs including chlorpyrifos-oxon, paraoxon, and echothiophate (ETP) have been commonly used by scientists as model compounds to evaluate cholinesterase-OP compound interactions. In contrast to nerve agents, however, chlorpyrifos-oxon, paraoxon, and ETP all have two ethoxy side chains attached to phosphorus, and thus the phosphorus atom does not possess a center of chirality. Most nerve agents, including both G- and V-type agents such as sarin (GB), soman (GD), cyclosarin (GF), *S*-[2-(diisopropylamino)ethyl]-*O*-ethyl methylphosphonothioate (VX), and Russian VX (VR), possess a center of chirality about phosphorus resulting in both S_p and R_p isomers. GD also has a chiral center at a carbon in the pinacolyl side chain. These nerve agents have shown significant stereoselective inhibition toward AChE and BChE. The S_p -enantiomers are significantly more potent inhibitors than their R_p -counterparts (4-8). Stereoselectivity for both AChE and BChE is determined by different steric interference encountered by the different enantiomers.

Enzyme-mediated detoxification of OPs has been a challenging goal for many years (for review see (9,10)). The objective is to identify enzymes or enzyme variants that can act as bioscavengers by converting the toxic OP compounds to non-toxic materials. Catalytic efficiency and substrate specificity are two defining parameters required for these bioscavengers. For AChE and BChE, because the wild type enzymes were irreversibly inhibited by OPs, efforts were focused on evolving spontaneous catalytic efficiency (11,12), or enhancing oxime-mediated enzyme reactivation (13,14). For other candidate detoxification enzymes with intrinsic OP compound hydrolysis activity, the approach was to ensure that the substrate specificities for nerve agents are comparable to the primary physiological target, AChE. Bacterial phosphotriesterase (5,15) and mammalian paraoxonase (16,17) were found to hydrolyze the R_p isomers GF and GD more efficiently than their respective S_p isomers. Therefore, it is essential to consider stereoselectivity as a key parameter during any detoxification bioscavenger development program. Such an effort includes maintaining correct stereoselectivity for variants of AChE and/or BChE, and elaboration of the correct substrate stereoselectivity for variants of detoxification catalysts such as phosphotriesterase and paraoxonase (5,15,16). Nerve agent model compounds with defined centers of chirality that mimic the most potent nerve agent structures are therefore essential tools for developing new detoxification catalysts.

Methylphosphonothioates are a class of nerve agent model compounds that have been synthesized in enantiomeric form and used to address cholinesterase stereoselectivity questions. A collection of methylphosphonothioates were initially synthesized by the Berman group to study *Torpedo* AChE inhibition (18). Later, related compounds were used to study inhibition of mouse AChE/BChE, and reactivation of their phosphorylated conjugates (13, 19,20). We synthesized two series of G-type nerve agent model compounds in enantiomerically enriched form. The compounds contained the same substituents on the phosphorus as the authentic G-type agents, but used thiomethyl ($\text{CH}_3\text{-S-}$) or thiocholine ($(\text{CH}_3)_3\text{NCH}_2\text{CH}_2\text{-S-}$) groups in place of the normal nerve agent leaving groups (i.e., fluoro for GB, GD, and GF; and

cyano for GA). In this study, we examined the inhibition kinetics of these nerve agent model compounds with both human AChE and human BChE. The synthetic compounds showed the anticipated stereoselective inhibition of human AChE and BChE as measured by bimolecular rate constants (i.e., $S_p > R_p$) and will be useful tools for evaluating candidate bioscavenger enzyme variants for nerve agent inhibition stereoselectivity.

Experimental Procedures

Toxicity warning

The nerve agent model compounds synthesized for this study are toxic and should be handled with extreme care. In addition, the thiomethyl analogs are volatile and should be handled in a well-ventilated area. All wastes containing the analogs were hydrolyzed by overnight incubation with 2.5 M NaOH and 10% ethanol before disposal.

Chemical and biological reagents

Methylphosphonothioic dichloride was obtained from Digital Specialty Chemicals, Ltd. (Toronto, Canada). Recombinant human AChE, β -lactoglobulin from bovine milk, acetylthiocholine iodide (ATCh), butyrylthiocholine iodide (BTCh), and 5,5'-dithiobis(2-nitrobenzoic acid) (DTNB) were purchased from Sigma-Aldrich Chemical Co. (St Louis, MO). Buffers and solvents were purchased from VWR Scientific, Inc. (San Diego, CA) in the highest purity commercially available. Highly purified human BChE and ETP were generously provided by Dr. Lockridge (University of Nebraska Medical Center, Omaha, NE).

Chemical synthesis

The synthetic route followed the procedures described previously (18,21,22) and illustrated briefly in Scheme 1 and 2. For chemical synthesis verification, ^1H - and ^{31}P -NMR spectra were recorded at ambient temperature at 500 MHz or 300 MHz and 200 MHz or 75 MHz, respectively, on a Varian Unity 500 or Varian Mercury 300 spectrometer (Varian, Inc., Walnut Creek, CA). Chemical shifts were reported in ppm relative to the residual solvent peak on the δ scale (CDCl_3 , ^1H : $\delta = 7.26$ and CD_3OD , ^1H : $\delta = 3.31$). Abbreviations for multiplicity include: br = broad, s = singlet, d = doublet, t = triplet, q = quartet, and m = multiplet. Coupling constants (J) were reported in Hertz (Hz). Optical rotations were measured on a Jasco P-1010 polarimeter (Jasco, Easton, MD). The specific rotation for a molecule (denoted $[\alpha]_D^{25}$) was given by the equation $[\alpha]_D^{25} = \alpha / (c \cdot l)$, where the concentration (c) was given in g mL^{-1} and the tube length (l) was 1 dm. Low resolution mass spectra were obtained on a Hitachi M-8000 mass spectrometer (Hitachi High-Technologies Co., Tokyo, Japan) using either positive or negative mode electrospray ionization. Preparative (PTLC) and analytical thin-layer chromatography (TLC) were done using 1 and 0.25 mm silica gel 60 (F254 Merck) plates, respectively, and visualized at 254 nm. Alternatively or in tandem, analytical TLC plates were visualized by treatment with phosphomolybdic acid or cerium molybdate solutions followed by heating.

Synthesis of (2*S_p*, 4*R*, 5*S*) and (2*R_p*, 4*R*, 5*S*)-trimethyl-5-phenyl-1, 3, 2-oxazaphospholidine-2-thione (14-*S_p* and 14-*R_p*) (Scheme 1)

A solution of methylphosphonothioic dichloride **12** (10 g, 49.6 mmol) in toluene (40 mL) was added slowly to a solution of (+)-ephedrine hydrochloride **13** (7.4 g, 49.6 mmol) dissolved in toluene (260 mL) and triethylamine (50 mL). The mixture was stirred at room temperature overnight. The mixture was then filtered through Celite to remove triethylamine hydrochloride salt. The filtrate was washed with water (2 times), dried over anhydrous sodium sulfate, and concentrated *in vacuo*. The crude mixture of diastereomers was purified by silica gel column chromatography (hexanes/ethyl acetate, 9:1, v:v) to yield 2.0 g (white solid, 17%) of **14-*S_p***

followed by 1.5 g (white solid, 13%) of **14-R_p**. The enantiomers **14-S_p** and **14-R_p** were verified as follows: (**14-S_p**), ¹H-NMR (300 MHz, CDCl₃) δ: 7.27-7.39 (m, 5H), 5.67 (dd, *J* = 5.9, 2.3 Hz, 3H), 3.63 (apparent septet, 1H), 2.77 (d, *J* = 12.1 Hz, 3H), 2.07 (d, *J* = 14.6 Hz, 3H), 0.75 (d, *J* = 6.6 Hz, 3H); [*a*]_D²⁵ +120.3° (*c* 0.052, CH₃OH); and (**14-R_p**), ¹H-NMR (300 MHz, CDCl₃) δ: 7.29-7.40 (m, 5H), 5.48 (dd, *J* = 5.6, 3.4 Hz, 3H), 3.63 (m, 1H), 2.68 (d, *J* = 12.7 Hz, 3H), 1.95 (d, *J* = 14.0 Hz, 3H), 0.82 (d, *J* = 6.3 Hz, 3H); [*a*]_D²⁵ +15.2° (*c* 0.054, CH₃OH).

General preparation of *R_p*- and *S_p*-alkylthiophosphonic acids (**15-17**) (Scheme 1)

A 1:1 mixture by volume of the requisite alcohol (ROH = **a**: isopropanol, **b**: cyclohexanol, **c**: 3,3-dimethyl-2-butanol) saturated with anhydrous hydrogen chloride and 2-butanone (3 mL) was added to individual solutions of **14** (*S_p* or *R_p*, 500 mg, 2.1 mmol) in 2-butanone (3.5 mL) at 0 °C. The reaction mixture was allowed to warm to room temperature and was stirred for 1 hour. The mixture was then poured into 10% (w/v) aq. sodium carbonate (12.5 mL), diluted with water (25 mL) and ethanol (40 mL). Pd/C (50 mg) was added and the reaction mixture was stirred under an atmosphere of H₂ gas overnight at room temperature. The mixture was then flushed with N₂ gas, filtered, and concentrated to remove the ethanol. The remaining aqueous mixture was diluted with water (10 mL) and extracted with diethyl ether (30 mL, 3 times). The organic layer was discarded. The aqueous layer was then acidified to pH < 3 with citric acid and extracted with 4:1 chloroform/isopropyl alcohol (15 mL, 5 times). The organic layer was dried over anhydrous sodium sulfate. Sodium sulfate was removed by filtration, and the filtrate was concentrated *in vacuo* to afford **15-17** as a clear viscous oil with the following yield: (**15-S_p**), 200 mg (63%); (**15-R_p**), 225 mg, (71%); (**16-S_p**), 270 mg (67%); (**16-R_p**), 313 mg (78%); (**17-S_p**), 152 mg (37%); and (**17-R_p**), 352 mg (86%). The crude product was used without further purification post NMR verification: (**15**), ¹H-NMR (300 MHz, CDCl₃) δ: 7.70 (br s, 1H), 4.78 (septet, *J* = 6.0 Hz, 1H), 1.70 (d, *J* = 15.0 Hz, 3H), 1.25 (apparent triplet, *J* = 6.0 Hz, 6H); (**16**), ¹H-NMR (300 MHz, CDCl₃) δ: 8.11 (br s, 1H), 4.50 (m, 1H), 1.88 (m, 2H), 1.73 (d, *J* = 15.0 Hz, 3H), 1.19-1.63 (m, 8H); and (**17**), ¹H-NMR (300 MHz, CDCl₃) (2:1 mixture of diastereomers, major diastereomer) δ: 5.13 (br s, 1H), 4.33-4.43 (m, 1H), 1.70 (d, *J* = 15.0 Hz, 3H), 1.22 (apparent triplet, *J* = 6.0 Hz, 3H), 0.89 (s, 9H); (minor diastereomer, diagnostic peaks) δ: 1.77 (d, *J* = 15.0 Hz, 3H), 1.09 (apparent triplet, *J* = 6.0 Hz, 3H), 0.9 (s, 9H).

General preparation of *R_p*- and *S_p*-*O*-alkyl *S*-methyl methylphosphonothioates (**5-7**) (Scheme 1)

The crude thiophosphonic acid [(**15-S_p**), 200 mg; (**15-R_p**), 225 mg; (**16-S_p**), 270 mg; (**16-R_p**), 313 mg; (**17-S_p**), 152 mg; and (**17-R_p**), 352 mg.] was directly dissolved in 10% (w/v) aqueous sodium carbonate (2.5 mL) and ethanol (10 mL). An excess of iodomethane (0.5 mL, 8.3 mmol) was added. The system was protected from light, and the reaction mixture was stirred at room temperature overnight. The reaction was worked up by diluting the mixture with water and extracting with methylene chloride (3-5 times). The organic layers were combined, dried over anhydrous sodium sulfate, and concentrated *in vacuo* under light vacuum (400 torr) at mild temperature (~35 °C). The crude product was purified by silica gel PTLC to provide the final product. The overall yield and compound verification are as follows: (**5-S_p**), PTLC (100% ether) afforded 18 mg of a liquid (13%); (**5-R_p**), yielded 25 mg of a liquid (18%); (**5**), ¹H-NMR (500 MHz, CDCl₃) δ: 4.76-4.84 (m, 1H), 2.31 (d, *J* = 12.9 Hz, 3H), 1.77 (d, *J* = 15.5 Hz, 3H), 1.38 (dd, *J* = 6.3, 26.6 Hz, 6H); ³¹P-NMR (200 MHz, CDCl₃) δ: 53.9; (**6-S_p**), silica gel PTLC (ether/hexanes 4:1) afforded 54 mg of a liquid (31%); (**6-R_p**), yielded 26 mg of a liquid (15%); (**6**), ¹H-NMR (500 MHz, CDCl₃) δ: 4.46-4.53 (m, 1H), 2.3 (d, *J* = 12.9 Hz, 3H), 1.90-2.01 (m, 1H), 1.9-1.93 (m, 1H), 1.77 (d, *J* = 15.5 Hz, 3H), 1.69-1.78 (m, 2H), 1.45-1.57 (m, 3H), 1.29-1.38 (m, 2H), 1.17-1.25 (m, 1H); ³¹P-NMR (200 MHz, CDCl₃) δ: 53.8; (**7-S_p**), silica gel PTLC (ether/dichloromethane 1:1, v:v) afforded 27 mg of a liquid (15%); (**7-R_p**), yielded 12

mg of a liquid (7%); (**7**), $^1\text{H-NMR}$ (500 MHz, CDCl_3) major diastereomer δ : 4.26-4.32 (m, 1H), 2.34 (d, $J = 12.9$ Hz, 3H), 1.78 (d, $J = 15.5$ Hz, 3H), 1.37 (dd, $J = 6.3, 11.5$ Hz, 6H), 0.90 (s, 9H); $^{31}\text{P-NMR}$ (200 MHz, CDCl_3) δ : 54.1; minor diastereomer, diagnostic peaks δ : 4.34-4.40 (m, 1H), 2.31 (d, $J = 12.9$ Hz, 3H), 1.77 (d, $J = 15.5$ Hz, 3H), 1.32 (dd, $J = 6.3, 10.8$ Hz, 6H), 0.92 (s, 9H); $^{31}\text{P-NMR}$ (200 MHz, CDCl_3) δ : 53.5. Single peak was observed for $^{31}\text{P-NMR}$ analysis of **5-7**.

General preparation of R_p and S_p *O*-alkyl *S*-dimethylaminoethyl methylphosphonothioates (**18-20**) (Scheme 1)

To the corresponding thiophosphonic acid **15-17** (**15- S_p** : 300 mg, 1.95 mmol, **15- R_p** : 313 mg, 2.03 mmol, **16- S_p** : 346 mg, 1.78 mmol, **16- R_p** : 419 mg, 2.16 mmol, **17- S_p** : 382 mg, 1.95 mmol, **17- R_p** : 447 mg, 2.28 mmol) in ethanol (5 mL) and 10% (w/v) aq. sodium carbonate (8 mL) was added (2-iodoethyl)dimethylamine hydroiodide (1.0 equiv). The reaction mixture was stirred at room temperature overnight. The mixture was then poured into saturated aqueous sodium chloride solution and extracted into dichloromethane. The organic layer was concentrated to yield a crude oil that was purified by silica gel flash column chromatography (0-30% (v/v) methanol in dichloromethane v:v, Teledyne ISCO CombiFlash Rf system, Newark, DE) to afford **18-20** as clear oils. The overall yield and compound verification are as follows: (**18- S_p**) 140 mg (32%), (**18- R_p**) 178 mg (39%), (**19- S_p**) 149 mg (32%), (**19- R_p**) 210 mg (43%), (**20- S_p**) 130 mg (25%), (**20- R_p**) 178 mg (34%); (**18**), $^1\text{H-NMR}$ (500 MHz, CDCl_3) δ : 4.72-4.78 (m, 1H), 2.90-3.01 (m, 2H), 2.54-2.62 (m, 2H), 2.26 (s, 6H), 1.75 (d, $J = 15.8$ Hz, 3H), 1.30 (dd, $J = 6.3, 30.6$ Hz, 6H); $^{31}\text{P-NMR}$ (200 MHz, CDCl_3) δ : 53.1; R_f (9:1 CH_2Cl_2 : CH_3OH) = 0.35; (**19**), $^1\text{H-NMR}$ (500 MHz, CDCl_3) δ : 4.50-4.43 (m, 1H), 2.89-3.03 (m, 2H), 2.57-2.66 (m, 2H), 2.28 (s, 6H), 1.93-1.99 (m, 1H), 1.86-1.91 (m, 1H), 1.77 (d, $J = 15.8$ Hz, 3H), 1.67-1.74 (m, 2H), 1.42-1.56 (m, 3H), 1.27-1.36 (m, 2H), 1.15-1.24 (m, 1H); $^{31}\text{P-NMR}$ (200 MHz, CDCl_3) δ : 53.0; R_f (9:1 CH_2Cl_2 : CH_3OH) = 0.34; (**20**), $^1\text{H-NMR}$ (500 MHz, CDCl_3) (major diastereomer) δ : 4.25-4.32 (m, 1H), 2.95-3.12 (m, 2H), 2.64-2.74 (m, 2H), 2.34 (s, 6H), 1.79 (d, $J = 15.8$ Hz, 3H), 1.34 (d, $J = 6.3$ Hz, 3H), 0.89 (s, 9H); (minor diastereomer's diagnostic peaks) δ : 4.30-4.35 (m, 1H), 1.28 (d, $J = 6.6$ Hz, 3H), 0.91 (s, 9H); $^{31}\text{P-NMR}$ (200 MHz, CDCl_3) δ : 53.3; R_f (9:1 CH_2Cl_2 : CH_3OH) = 0.32.

General synthesis of R_p and S_p 2-(*O*-alkyl(methyl)phosphorylthio)-*N,N,N*-trimethylethanaminium iodide (**8-10**) (Scheme 1)

To a solution of **18-20** (**18- S_p** : 70 mg, 0.31 mmol, **18- R_p** : 60 mg, 0.27 mmol, **19- S_p** : 35 mg, 0.13 mmol, **19- R_p** : 30 mg, 0.11 mmol, **20- S_p** : 6 mg, 0.02 mmol, **20- R_p** : 6 mg, 0.02 mmol) in benzene (1 mL) was added iodomethane (1 mL). This solution was allowed to stand at room temperature overnight and then concentrated and dried under high-vacuum to afford pure **8-10** as clear-light yellow oils. The overall yield and compound verification were as follows: (**8- S_p**) 109 mg (96%), (**8- R_p**) 69 mg (70%), (**9- S_p**) 50 mg (94%), (**9- R_p**) 10 mg (22%), (**10- S_p**) 6.5 mg (71%), (**10- R_p**) 5.8 mg (63%); (**8**), $^1\text{H-NMR}$ (500 MHz, CD_3OD) δ : 4.79-4.82 (m, 1H), 3.62-3.69 (m, 2H), 3.25-3.32 (m, 2H), 3.19 (s, 9H), 1.91 (d, $J = 20.0$ Hz, 3H), 1.37 (dd, $J = 20.0, 5.0$ Hz, 3H); $^{31}\text{P-NMR}$ (200 MHz, CD_3OD) δ : 54.6; (**9**), $^1\text{H-NMR}$ (500 MHz, CD_3OD) δ : 4.49-4.55 (m, 1H), 3.61-3.69 (m, 2H), 3.21-3.32 (m, 2H), 3.18 (s, 9H), 1.9-1.96 (2H), 1.92 (d, $J = 15.0$ Hz, 3H), 1.74-1.76 (m, 2H), 1.53-1.58 (m, 3H), 1.26-1.41 (m, 3H); $^{31}\text{P-NMR}$ (200 MHz, CD_3OD) δ : 54.7; (**10**), $^1\text{H-NMR}$ (500 MHz, CD_3OD) major diastereomer δ : 4.31-4.37 (m, 1H), 3.59-3.68 (m, 2H), 3.22-3.32 (m, 2H), 3.18 (s, 9H), 1.93 (d, $J = 15.0$ Hz, 3H), 1.32-1.39 (m, 3H), 0.92 (apparent t, $J = 10.0$ Hz, 9H); $^{31}\text{P-NMR}$ (200 MHz, CD_3OD) δ : 54.9. Single peak was observed for $^{31}\text{P-NMR}$ analysis of **8-10**.

Synthesis of (2*R_p*, 4*R*, 5*S*) and (2*S_p*, 4*R*, 5*S*)-chlorodimethyl-5-phenyl-1, 3, 2-oxazaphospholidine-2-thione (22-*R_p* and 22-*S_p*) (Scheme 2)

A solution of thiophosphoryl chloride **21** (4.2 mL, 41 mmol) in toluene (25 mL) was slowly added to a slurry of (+)-ephedrine **13** (8.60 g, 43 mmol) and triethylamine (35 mL) in toluene (150 mL). The mixture was stirred at room temperature overnight and then poured into ethyl acetate and washed with water (3 times). The organic layer was dried over anhydrous sodium sulfate. Sodium sulfate was removed by filtration, and the filtrate was concentrated *in vacuo* to afford a yellow oil that solidified upon standing. The crude material was found to be a 1:3 mixture of the *R_p*:*S_p* isomers. Purification of the crude mixture of diastereomers consisted of passing the material through a silica column (4 inch height by 3 inch diameter) using dichloromethane as eluent followed by silica gel flash column chromatography (0-10% ethyl acetate/hexanes, v:v) to give 1.6 g (15%) of **22-*R_p*** (top spot) and 5.52 g (53%) of **22-*S_p*** (bottom spot). The compounds were verified by ¹H-NMR analysis: (**22-*R_p***), ¹H-NMR (300 MHz, CDCl₃) δ: 7.30-7.44 (m, 5H), 5.83 (d, *J* = 6.6 Hz, 1H), 3.83 (dq, 1H), 2.92 (d, *J* = 14.6 Hz, 3H), 0.88 (d, *J* = 6.9 Hz, 3H); and (**22-*S_p***), ¹H-NMR (300 MHz, CDCl₃) δ: 7.32-7.41 (m, 5H), 5.60 (t, 7.3 Hz, 1H), 3.75 (sextet, *J* = 6.0 Hz, 1H), 2.73 (d, *J* = 16.8 Hz, 3H), 0.80 (d, *J* = 6.6 Hz, 3H).

Synthesis of (2*S_p*, 4*R*, 5*S*) and (2*R_p*, 4*R*, 5*S*)-*N,N*-dimethylamino-dimethyl-5-phenyl-1, 3, 2-oxazaphospholidine-2-thione (23-*S_p* and 23-*R_p*) (Scheme 2)

A solution of **22** (*S_p* or *R_p* isomer, 1.0 g, 3.82 mmol) in dry toluene (10 mL) in a pressure tube was bubbled with anhydrous dimethylamine gas. After 1 minute, the tube was sealed and stirred at room temperature. After 4 hours, the mixture was filtered through Celite to remove the dimethylamine hydrochloride salt. The filtrate was diluted with ethyl acetate, and washed with water (2 times). The organic layer was dried over anhydrous sodium sulfate. Sodium sulfate was removed by filtration, and the filtrate was concentrated *in vacuo* to afford **23-*S_p*** (1.03 g, 100%) or **23-*R_p*** (1.03 g, 100%) as a yellow oil. The crude material was used without further purification. The compounds (**23-*S_p*** and **23-*R_p***) were verified by ¹H-NMR analysis: ¹H-NMR (300 MHz, CDCl₃) δ: 7.28-7.38 (m, 5H), 5.67 (d, *J* = 6.9 Hz, 1H), 3.53 (sextet, *J* = 6.0 Hz, 1H), 2.95 (s, 3H), 2.91 (s, 3H), 2.60 (d, *J* = 11.8 Hz, 3H), 0.75 (d, *J* = 6.6 Hz, 3H).

Synthesis of *S_p* and *R_p* *O*-ethyl *O*-hydrogen dimethylphosphoramidothioate (24-*S_p* and 24-*R_p*) (Scheme 2)

To a solution of **23-*S_p*** (500 mg, 1.85 mmol) or **23-*R_p*** (503 mg, 1.86 mmol) in absolute ethanol (2 mL) was added a solution of ethanol (2 mL) saturated with hydrogen chloride. After stirring at room temperature for 2 hours, the mixture was basified to pH~12 with aq. sodium hydroxide (10 N) and stirred at room temperature overnight. The mixture was extracted with diethyl ether (3 times). The organic layer was discarded and the aqueous layer acidified to pH < 3 with citric acid and extracted with 4:1 chloroform/isopropyl alcohol (3 times). The organic layer was dried over anhydrous sodium sulfate. Sodium sulfate was removed by filtration, and the filtrate was concentrated *in vacuo* to afford **24-*S_p*** (308 mg, 98%) or **24-*R_p*** (315 mg, 100%) as a clear viscous oil. The crude material was used without further purification. The compounds (**24-*S_p*** and **24-*R_p***) were verified by ¹H-NMR analysis: ¹H-NMR (300 MHz, CD₃OD) δ: 3.60 (quart, *J* = 7.5 Hz, 2H), 2.82 (s, 3H), 2.79 (s, 3H), 1.32 (t, *J* = 7.5 Hz, 3H).

Synthesis of *S_p* and *R_p* 2-((dimethylamino)(ethoxy)phosphorylthio)-*N,N,N*-trimethylethanaminium iodide (11-*S_p* and 11-*R_p*) (Scheme 2)

To a solution of **24-*S_p*** (645 mg, 3.81 mmol) or **24-*R_p*** (315 mg, 1.86 mmol) in ethanol (10 mL) and 10% (w/v) aq. sodium carbonate (10 mL) was added (2-iodoethyl)dimethylamine hydroiodide (1.0 equiv.). The reaction mixture was stirred at room temperature overnight and then poured into saturated aqueous sodium chloride solution and extracted with

dichloromethane (3 times). The organic layer containing (*S*)-*S*-2-(dimethylamino)ethyl *O*-ethyl dimethylphosphoramidothioate (**25-S_p** or **25-R_p**) was concentrated to ~3 mL then diluted with benzene (3 mL) and excess methyl iodide (3 mL) was added. The mixture was allowed to stand without stirring at room temperature overnight. The solid precipitate **11-S_p** (127 mg, 9%) or **11-R_p** (67 mg, 9%) was collected by decanting the liquid and drying under high vacuum. The compounds (**11-S_p** and **11-R_p**) were verified as follows: ¹H-NMR (500 MHz, CD₃OD) δ: 4.12-4.20 (m, 4H), 3.76 (t, *J* = 9.0 Hz, 2H), 3.34 (s, 9H), 2.78 (s, 3H), 2.74 (s, 3H), 1.36 (t, *J* = 9.0 Hz, 3H); ³¹P-NMR (200 MHz, CDCl₃) δ: 35.7; (**11-S_p**), [*a*]_D²⁵ +20.7° (c. 0.0075, CH₃OH); (**11-R_p**), [*a*]_D²⁵ -20.1° (c. 0.0072, CH₃OH). Single peak was observed for ³¹P-NMR analysis of **11**.

Stability test

The stability of the OP analogs bearing the thiocholine leaving group for GB, GD, GF, and GA (i.e., **8-11**) was analyzed. The compounds were dissolved in 50 mM potassium phosphate buffer pH 7.2 at 0.5-1 mg mL⁻¹, and the samples were kept at room temperature shielded from direct light. Aliquots were taken at selected time points and incubated with the Ellman reagent to detect buffer-mediated hydrolysis. The half-life of each compound was calculated from the molar extinction coefficient of 13,600 M⁻¹cm⁻¹ (23).

Enzyme assays

AChE and BChE activities were measured spectrophotometrically (Lambda 25, Perkin-Elmer, Palo Alto, CA) with an Ellman assay (23). Briefly, ATCh or BTCh was used as substrate for AChE and BChE, respectively, at 1 mM final concentration. The incubations were carried out in 50 mM potassium phosphate buffer (pH 7.2) at 25°C in the presence of 0.2 mM DTNB. Hydrolysis was monitored continuously by absorbance at 412 nm. Functional activity was calculated from the molar extinction coefficient of 13,600 M⁻¹cm⁻¹ (23).

Determination of inhibition rate constants (*k_i*) for AChE and BChE

Because some of the *R_p* isomers from the thiomethyl analogs have low inhibition potencies for the cholinesterases, long-term incubation periods were needed to reliably determine the inhibition constants. To prevent loss of cholinesterase enzyme activity during incubation, 30 µg mL⁻¹ of bovine milk β-lactoglobulin were included in the enzyme-inhibitor incubation mixture. Nerve agent model compounds were solubilized in acetonitrile (thiomethyl analogs) or DMSO (thiocholine analogs) and then diluted in H₂O before use. Final solvent concentration in the inhibition mixtures was < 5%. Control experiments observed no impact on enzyme activity with < 5% solvent in the incubation mixture (i.e., BChE or AChE incubated with 30 µg mL⁻¹ bovin milk β-lactoglobulin in 10 mM Tris buffer pH 7.6 at 25°C plus <5% acetonitrile or DMSO). Inhibition was initiated by mixing 3.6 × 10⁻³ IU of highly purified BChE or AChE with various amounts of each nerve agent analog (i.e., **5-11**) in 30 µL final reaction volume in 10 mM Tris buffer pH 7.6. The inhibition mixtures were incubated at 25°C, and at defined times, 970 µL of reaction mixture was added to determine residual cholinesterase activity at 25°C as described above. For kinetic studies, five to seven concentrations of analog were used, and at least four time points of inhibition were taken for each concentration. Plots of ln(residual cholinesterase activity) versus incubation time afforded *k_{app}* (the apparent first order rate constant for inhibition at a given concentration of analog). A re-plot of the *k_{app}* versus the concentration of the nerve agent analog afforded the inhibition constant values. For hyperbolic re-plots, non-linear curve fitting to the equation $k_{app} = k_2[OP]/(K_D + [OP])$ afforded both phosphorylation rate constants *k₂* and equilibrium dissociation constants *K_D* (24). Bimolecular rate constants *k_i* were calculated from the ratio of the *k₂*/*K_D*. For linear re-plots, bimolecular rate constants *k_i* were determined by linear regression analyses of the slope.

Molecular Docking Simulations

The thiomethyl analogues were optimized using Becke's three-parameter hybrid exchange functional with the Lee-Yang-Parr correlation functional (B3LYP) (25-27) method in conjunction with the 6-31+G* basis set in the Gaussian03 (28) suite of programs (29). The atomic charges were calculated using the CHarges from Electrostatic Potential Grid (CHELPG) (30) method as implemented in Gaussian03. Docking simulations for all of the thiomethyl analogues were carried out with the crystal structure of human BChE (PDB ID: 1P0I) (31) and with the aid of the AutoDock 4.0 program (32). The OP analogues as well as a few selected residues of BChE – namely, F329, Y332 and W82, of which F329 and Y332 residues are at the mouth of the gorge while W82 is the cation- π interaction site – were treated as flexible residues during these docking simulations. All of the non-polar hydrogens were merged before performing the grid calculations for the docking protocol. The grid box covered the entire gorge and surroundings of the active site, and was of $60 \times 60 \times 60 \text{ \AA}^3$ volume with the grid spacing of 0.2972 \AA . A total of 2,500,000 energy evaluations with 250,000 generations were used along with a total of 200 standard genetic algorithm docking simulations for each of the analogues. The preparation for human AChE (PDB ID: 1B41) (33) was carried out with slightly modified parameters. A smaller grid was created, of dimensions $50 \times 50 \times 50 \text{ \AA}^3$, and with a slightly finer spacing of 0.275 \AA . A total of 200 genetic docking simulations were carried out for each of the model compounds.

Data Analysis

All linear and non-linear regression analyses were done with Graphpad Prism Programs (Version 3.00, Graphpad, Inc., La Jolla, CA). Best fit values and standard errors are presented.

Results

Chemical Synthesis

The structures of the nerve agent model compounds synthesized for this study are shown in Table 1. The synthetic route followed the procedures described previously (18,21,22). Schemes 1 and 2 illustrated the synthesis of enantiomerically enriched S_p isoforms. Synthesis of the corresponding R_p isomers followed the same synthetic scheme using alternative diastereomeric intermediates (i.e., **14- R_p** in Scheme 1 and **22- S_p** in Scheme 2). The synthetic method utilized (+)-ephedrine to form a diastereomeric mixture at the phosphorus center of chirality that was separable by silica gel column chromatography. The identification of the phosphorus diastereomers (S_p or R_p) was done by comparison of the $^1\text{H-NMR}$ spectra to the literature report (18). Each diastereomer was then taken forward to form the nerve agent analog that was enantiomerically-enriched about the phosphorus center. 2-Iodo-*N,N*-dimethylethanamine hydroiodide (**34**) was used as the alkylating reagent for the synthesis in the thiocholine analogs (i.e., **8-11**). The pinacolyl alcohol used to synthesize **7** and **10** was a racemic mixture and resulted in a diastereomeric carbon center (S_c and R_c) in **7** and **10**. Phosphorus isomers **7- S_p** and **10- S_p** consisted of a mixture of S_pS_c and S_pR_c forms, and similarly **7- R_p** and **10- R_p** analogs were mixtures of R_pS_c and R_pR_c forms. **5** and **7** have been reported previously (18), while the remaining 10 analogs are novel. Analytically pure products were obtained by flash column chromatography, PTLC or filtration. Optical purity was analyzed for selected OP compounds. The common intermediates **14- S_p** and **14- R_p** provided match values to previously reported mirror image compounds (18). Compounds **11- S_p** and **11- R_p** exhibited equal and opposite optical rotations, substantiating the optical purity obtained during separation of the diastereomeric reactants. Spiking of **14- S_p** with 1% and 2% **14- R_p** was readily detected by $^1\text{H-NMR}$ analysis. This confirmed that $^1\text{H-NMR}$ analysis of compound **14- S_p** and **14- R_p** post chromatographic separation was a valid method to verify overall chemical purity as well as diastereomeric purity for **14- S_p** and **14- R_p** (data not shown). Because the separation of **14- S_p** and **14- R_p** was the only chiral separation step in the entire synthesis, we believe the

diastereomeric purity of **14-*S_p*** and **14-*R_p*** represented the enantiomeric purity of compounds *S_p* and *R_p* **5-10**, respectively.

The aqueous stability (pH = 7.4) of the OP analogs bearing the thiocholine leaving group for GB, GD, GF, and GA (i.e., **8-11**) indicated that with the exception of **8**, all compounds showed no detectable degradation after seven days in phosphate buffer. Compounds **8** showed a half-life of 57 hours under these conditions. The stability of the thiomethyl leaving group analogs was not extensively examined, however, overnight incubation in buffer conditions did not show any detectable level of hydrolysis.

Carrier proteins

The thiomethyl analogs were poor inhibitors of both AChE and BChE. Incubation times of up to 30 minutes were required to achieve acceptable levels of inhibition with these relatively low potency inhibitors. The long incubation times presented a technical problem. Significant decreases in the enzyme activities were observed after 30 minutes when control experiments were run in the absence of inhibitor. AChE lost 40% of its starting activity and BChE lost 32% (data not shown). Such loss of activity is commonly due to the adsorption of enzyme to the reaction vessel surface. Due to variable amounts of bovine serum BChE contamination in commercial preparations of bovine serum albumin, bovine serum albumin was not used in these assays. Ultimately, β -lactoglobulin from goat milk, at 30 $\mu\text{g mL}^{-1}$, was selected to protect the cholinesterases based on the following factors: 1) no detectable cholinesterase activity was associated with the commercial product; 2) no interference of either AChE or BChE inhibition by the analogs was observed based on comparable kinetics when highly potent analogs were tested in the presence and absence of the carrier protein, and 3) over 95% enzyme activity was retained for both AChE and BChE, after incubation for over 90 minutes in the presence of the carrier protein. Although the carrier protein was only needed for kinetic measurement of low potency inhibitors, it was included in all experiments to ensure comparable results for all assays.

Kinetic parameters for inhibition of AChE by the thiomethyl model compounds of GB, GF, and GD

To determine the kinetic parameters for phosphorylation by the different nerve agent analog stereoisomers, AChE was incubated with various concentrations of the analogs for different time periods. At the end of each incubation period, the enzyme inhibitor mixture was diluted 33-fold into the assay mixture to measure remaining cholinesterase hydrolysis activity. The activity of AChE decreased exponentially over the time course of the experiments. Apparent rate constants (k_{app}) for the inhibition were obtained from linear regression analysis of the semi-logarithmic plots of $\ln(\text{residual AChE activity})$ versus time of incubation (Figure 1). Replots of k_{app} versus inhibitor concentration showed saturation condition at higher OP analog concentrations (Figure 2A and 2B) to allow calculation of k_2 and K_D based on non-linear curve fitting analysis.

For human AChE, *S_p* isomers were substantially more potent inhibitors than *R_p* isomers with the second order inhibition constants in the 10^3 to $10^4 \text{ M}^{-1}\text{min}^{-1}$ range for *S_p* enantiomers, and in the 10^2 to $10^3 \text{ M}^{-1}\text{min}^{-1}$ range for *R_p* enantiomers (Table 2). The **6-*S_p*** provided the most significant stereoselectivity (i.e., 28-fold greater potency compared with **6-*R_p***), while approximately 10-fold stereoselectivity (*S_p/R_p*) was found for the **5** and **7** (Table 2). The greater potency of the *S_p* enantiomers for AChE was largely dependent on greater phosphorylation rates by the *S_p* analogs. The k_2 values for **5-*S_p***, **6-*S_p***, and **7-*S_p*** were greater than their corresponding *R_p* analogs by 20-, 7-, and 16-fold, respectively. The affinity of AChE for the analogs was greatest for **6-*S_p*** and lowest for **5-*S_p***. The affinity for all the *R_p* enantiomers was not significantly different. A ranking of the inhibition potency for the six compounds

determined on the basis of their second order inhibition rate constants was as follows: $6\text{-}S_p > 7\text{-}S_p > 6\text{-}R_p > 7\text{-}R_p \approx 5\text{-}S_p > 5\text{-}R_p$.

It is noteworthy that extrapolation of the inhibition time courses back to time zero did not result in a common intercept for inhibition by $7\text{-}S_p$ and $7\text{-}R_p$ (Figure 1E and 1F). Under normal circumstances, such an extrapolation would be expected to yield a common intercept that represented the initial, uninhibited activity of the enzyme. The extrapolated intercepts for these inhibitors fell below the uninhibited activity. Furthermore, the more inhibitor that was used in the incubation, the lower the extrapolated intercept became. Such behavior indicated that a portion of the AChE was being inhibited immediately upon mixing with the inhibitor. A similar pattern has been observed with studies for *Torpedo* AChE (18) and mouse AChE (35) using similar compounds. In both reports, the initial phase of complex formation was not investigated further. There are two common causes for such behavior. The first would be non-covalent complex formation between the inhibitor and AChE. This would require that the concentration of inhibitor, at the time of the assay, be comparable to the dissociation constant for the inhibitor-AChE complex. However, since the activity assay involved a 33-fold dilution of the inhibitor-AChE complex and the starting inhibitor concentration never saturated the non-covalent complex (see Figure 2A), it is unlikely that the non-covalent inhibitor-AChE complex was present to a significant extent in the activity assay. In addition, the assay conditions included an excess of substrate, which competed with the inhibitor for non-covalent binding to the AChE. Together, these conditions make a non-covalent inhibitor-AChE complex an unlikely choice to explain the zero time inhibition. An alternative possibility is rapid reaction with a contaminant in the analog preparation. Because the amount of the zero time inhibition appeared to be limited, at any given inhibitor concentration, the concentration of the rapid inhibitor would have to be less than the concentration of the enzyme at sub-stoichiometric conditions. Because the nominal concentration of the inhibitor was in the mM range, while the concentration of AChE was in the nM range, any rapidly reacting inhibitor must have been present at levels 10^{-6} -fold less than the principal inhibitor. As such, a very minor contaminant, but a very potent inhibitor may be operating to afford the results observed. Kinetic parameters for these analogs were determined using the slow linear phase portion of the reaction disregarding the initial complex formation.

Kinetic parameters for inhibition of BChE by the thiomethyl model compounds of GB, GD and GF

With the exception of $7\text{-}R_p$, all inhibition incubations for human BChE showed the same hyperbolic profile as that of AChE (Figure 2C and 2D). BChE inhibition by $7\text{-}R_p$ showed marked biphasic behavior, with a fast inhibition that was complete in the initial 15 seconds of incubation, followed by a very slow inhibition that could not be reliably measured. Kinetic parameters for $7\text{-}R_p$ were not reported, because measurement of the slow inhibition kinetics was unreliable. The initial, rapid inhibition was similar to the rapid, mixing time inhibition described for AChE. For the GB and GF model compounds, the S_p isomers consistently showed greater potency for BChE inhibition than the R_p isomers, with second order inhibition rate constants in the 10^2 to $10^4 \text{ M}^{-1}\text{min}^{-1}$ range for the S_p enantiomers and 10^1 to $10^2 \text{ M}^{-1}\text{min}^{-1}$ range for the R_p enantiomers (Table 2). $6\text{-}S_p$ provided 47-fold greater inhibition potency compared to the $6\text{-}R_p$. Both $5\text{-}S_p$ and $6\text{-}S_p$ showed greater k_2 values against BChE than their R_p counterparts. $6\text{-}S_p$ and $7\text{-}S_p$ showed comparable dissociation constants and were the two compounds with greatest inhibition potency toward BChE (Table 2). The overall rank order of the five compounds for BChE inhibition potency was $6\text{-}S_p > 7\text{-}S_p > 6\text{-}R_p \approx 5\text{-}S_p > 5\text{-}R_p$. The rank order is in agreement with the ranking described above for AChE.

Kinetic parameters for inhibition of AChE and BChE by thiocholine model compounds of GB, GF, GD, and GA

To extend the structure-activity relationship enzyme inhibition studies, a series of thiocholine-containing nerve agent model compounds were synthesized and studied (**8-11**, Table 1, Schemes 1 and 2). For all inhibition reactions examined except for **10-*R_p*** toward BChE, the activity of both AChE and BChE decreased exponentially with the time of incubation in the presence of the thiocholine analogs. Plots of $\ln(\text{residual cholinesterase activity})$ versus time of incubation were linear (data not shown). For **10-*R_p*** incubation with BChE, initial rapid inhibition similar to that described above for AChE was evident. A linear portion of the slow phase inhibition kinetics was used to obtain k_{app} . Replots of k_{app} versus inhibitor concentration were linear for all AChE incubations (Figure 3A, B) and most BChE incubations (Figure 3C). Linear curve fitting afforded bimolecular rate constants (k_i in Table 3). For reactions with BChE in the presence of *R_p* isomers of GB, GF, and GD model compounds, replots of k_{app} versus inhibitor concentration approached saturation (Figure 3D) and afforded k_2 and K_D values (Table 3). Bimolecular rate constant determined for the control compound ETP were $1.8 \times 10^6 \text{ M}^{-1}\text{min}^{-1}$ for AChE and $2.6 \times 10^6 \text{ M}^{-1}\text{min}^{-1}$ for BChE. These values were in good agreement with literature values of $1.5 \times 10^6 \text{ M}^{-1}\text{min}^{-1}$ for AChE (6) and $3.2 \times 10^6 \text{ M}^{-1}\text{min}^{-1}$ for BChE (36).

Compared with the thiomethyl analogs **5-7**, the thiocholine analogs **8-10** were much more potent inhibitors of both human AChE and BChE. The second order inhibition rate constants for the thiocholine analogs were in the range of 1×10^5 to $4 \times 10^7 \text{ M}^{-1}\text{min}^{-1}$ for the *S_p* enantiomers and 4×10^4 to $8 \times 10^5 \text{ M}^{-1}\text{min}^{-1}$ range for the *R_p* enantiomers (Table 3). The overall rank order of the eight compounds for AChE inhibition potency was $9\text{-}S_p > 8\text{-}S_p > 10\text{-}S_p > (9\text{-}R_p, 10\text{-}R_p, 8\text{-}R_p) > 11\text{-}S_p > 11\text{-}R_p$. The rank order for BChE inhibition potency was $9\text{-}S_p > 10\text{-}S_p > (11\text{-}S_p, 8\text{-}S_p) > (9\text{-}R_p, 8\text{-}R_p, 11\text{-}R_p) > 10\text{-}R_p$. The *S_p* enantiomers consistently showed greater potency for both AChE and BChE compared with the *R_p* enantiomers, with the greatest stereoselectivity being observed for $9\text{-}S_p > 9\text{-}R_p$ with 52-fold potency against AChE (Table 3). Compounds **11** showed less than 4-fold stereoselectivity for both AChE and BChE, and were the least potent pair of inhibitors against AChE. For reaction of **8-*R_p***, **9-*R_p***, **10-*R_p*** with BChE, equilibrium dissociation constants K_D were in the range of 4-11 μM (Table 3), a markedly greater affinity compared to the corresponding values for the thiomethyl analogs (Table 2).

Molecular docking simulations

Docking simulations of the thiomethyl analogues were done for optimal placing of the OP analogues into the catalytic gorge of human AChE and BChE (Figure 4 for compound **5** in BChE). Both **5-*S_p*** and **5-*R_p*** was found to have two binding orientations in BChE with either thiomethyl group (Figure 4A, 4C) or alkoxy group (Figure 4B, 4D) at the apical position. Based on the calculated binding free energy, the docking of **5-*S_p*** was more favorable than **5-*R_p***; and docking positions with alkoxy group at the apical position were slightly more favorable than the alternative positions for both **5-*S_p*** and **5-*R_p***. Similarly, docking of **6-*S_p*** and **7-*S_p*** in BChE showed both orientations, with alkoxy group at the apical position slightly more favorable. In the case of the docking simulations with **6-*R_p***, the binding orientations with a thiomethyl group at the apical position similar to that shown in Figure 4C was observed to be more favorable both statistically as well as energetically. This selective binding can be attributed to favorable van der Waals interaction of the cyclohexyl group with the residues that created the spacious acyl pocket of BChE. For **7-*R_p***, the binding orientation with the alkoxy group at the apical position similar to that shown in Figure 4D was dominantly favorable. An alternative position with the thiomethyl group at the apical position created unfavorable steric interaction as the bulky pinacolyl group lies under the acyl loop. Binding orientations were not identified for all OP analogues in AChE, making specific trends difficult to ascertain. However, the results for

6 and 7 suggest that for S_p isomers, orientations leading to P–S cleavage are more favorable than those leading to P–O cleavage.

Discussion

The potency for irreversible inhibition of the enantiomerically enriched thiomethyl and thiocholine analogs was determined for both human AChE and BChE to compare the stereoselectivity and overall inhibition potency. S_p and R_p forms of **5** and **8**, both GB model compounds, have been used in previous reports (18). They were prepared using chemical synthesis and purification procedures similar to those reported here. The potency of **5** against human BChE (Table 2) was comparable to that reported for *Torpedo* AChE (i.e., $317 \text{ M}^{-1}\text{min}^{-1}$ for **5- S_p** and $15 \text{ M}^{-1}\text{min}^{-1}$ for **5- R_p**) (18) and mouse AChE (i.e., $310 \text{ M}^{-1}\text{min}^{-1}$ for **5- S_p** and $1.7 \text{ M}^{-1}\text{min}^{-1}$ for **5- R_p**) (20). The potency for **8** against human AChE (Table 3) was comparable to that reported for *Torpedo* AChE ($1.3 \times 10^7 \text{ M}^{-1}\text{min}^{-1}$ for **8- S_p** and $0.87 \times 10^5 \text{ M}^{-1}\text{min}^{-1}$ for **8- R_p**) (18) and mouse AChE ($1.6 \times 10^7 \text{ M}^{-1}\text{min}^{-1}$ for **8- S_p** and $1.5 \times 10^5 \text{ M}^{-1}\text{min}^{-1}$ for **8- R_p**) (19). Chemical synthesis and inhibition kinetics for the other compounds described herein have not been reported previously.

The inhibition of cholinesterase by OPs occurs through nucleophilic attack of the active site serine on the phosphorus atom that results in the formation of a pentavalent, bipyramidal intermediate. The intermediate is not stable, and the functional group in the apical position opposite the serine detaches, yielding a phosphorylated enzyme adduct. From a chemical reactivity point of view, thiols are much more acidic than similar alcohols, with estimated pK_a values of 10 for RSH versus pK_a values of 16–19 for ROH (where R is a non-charged alkyl group). Therefore, thiolates are generally predicted to be better leaving groups than similar alkoxides. For the nerve agent model compounds being examined in this report, phosphorylation is predicted to release the thiomethyl group or the thiocholine group, yielding a phosphorylated enzyme adduct identical to those formed by the authentic nerve agents. The pK_a value of thiocholine is 7.8 (37), that is significantly lower than the pK_a of a thiomethyl group (10.4) due to the through space electron withdrawing nature of the ammonium cation present in the choline group. Thus, the thiocholine group makes a much better leaving group than the thiomethyl group. In addition to chemical reactivity, a previous report from Hosea *et al.* (20) showed that Asp74 in mouse AChE was essential for high potency inhibition of related thiocholine analogs. The study indicated that the thiocholine leaving group was oriented upward in the gorge of mouse AChE, pointing toward the peripheral anionic binding site (20). This position puts the thiocholine on the opposite side of the phosphorus from the attacking active site serine, which is essential for thiocholine to perform as a leaving group for phosphorylation. By comparison, the thiomethyl group lacks a positive charge and is substantially smaller than the thiocholine. These features enable the thiomethyl group to have less interaction with the peripheral anionic site to ensure correct positioning to function as a leaving group. Correlating the kinetic study with product formation characterization and molecular dynamic simulations confirmed these predictions.

Mass spectral analysis by Dr. Lockridge (38) examining the adducts formed from BChE during incubation with the nerve agent model compounds from Table 1 revealed that phosphorylation by the thiocholine analogs (i.e., **8**, **9**, and **10**) resulted in adducts that were the consequence of thiocholine release. However, for the thiomethyl analogs, only **6- S_p** and **6- R_p** yielded phosphorylated enzyme adducts that were the result of thiomethyl being the sole leaving group. In contrast, the GB and GD model compounds, **5** and **7**, released either the thiomethyl or the alkoxy group (i.e., isopropyl for **5**, and pinacolyl for **7**). As discussed above, thiocholine has a greater chemical propensity, and is better oriented in the protein to serve for leaving group phosphorylation. For the thiomethyl analogs, lack of a strong preference for the thiomethyl group enabled the alkoxy group to be a competitive leaving group. Such a rationalization could

explain why a single adduct was formed by thiocholine analogs while a mixture of adducts was formed by the thiomethyl phosphonates (40).

To understand the impact of multiple complex formations for **5** and **7** on inhibition kinetics, a kinetic model was built to describe the events (data not shown). The model predicted no biphasic nature for the inhibition kinetics under the first-order assay conditions employed in this study. The inhibition potency reported here for **5** and **7** represents the combined apparent inhibition potency contributed from both complexes. Even though molecular dynamics is limited in offering explanations for kinetic events because the simulation studies only examined the pre-dissociative complexes and do not consider transition states and other kinetic events, the study still offered many clues explaining the kinetic observations. Based on molecular dynamic analysis, the two docking positions give comparable energy values suggesting similar binding affinity, explaining why the derived apparent K_D values for **5-S_p** and **5-R_p** are not significantly different. Molecular dynamic studies also indicated that for both **5-R_p** and **7-R_p**, docking orientations with alkoxy groups positioned as leaving groups are more favorable. This suggested that the apparent k_2 values for **5-R_p** and **7-R_p** are affected to a greater extent by the P-O cleavage event, rendering lower k_2 values for the R_p isoform. Alternative binding orientations and inhibition mechanisms have been characterized comprehensively for the (1*R*)- and (1*S*)-isomalathion stereoisomers to reveal different primary leaving groups and subsequent aging mechanism (39,40). The thiomethyl analogs examined here exhibited more flexibility in the catalytic site and allowed both binding orientations to yield phosphorylated adducts.

With regard to stereoselectivity of inhibition, the results showed that for both the thiomethyl and the thiocholine analogs reacting with either AChE or BChE, there is a pronounced stereoselective preference for the S_p analog over its R_p counterpart. The extent of that preference varied depending on the analog pair examined as well as the enzyme target. In AChE, the acyl binding pocket is a small space that was designed to accommodate the methyl group of the acyl moiety of the substrate. The space would be suitable for the methyl group of nerve agents or of the model compounds reported here, but not for large alkoxy groups. For the thiocholine analogs in this study, if the phosphoryl oxygen was fixed in the oxyanion hole and the thiol leaving group was oriented upward in the gorge, then either the methyl or the alkoxy group would have to be placed in the acyl binding pocket depending on the stereochemistry of the analog. A S_p stereoisomer that placed a methyl group in the acyl pocket would be expected to fit much better than an R_p stereoisomer that places a bulky alkoxy group into this position. This prediction is confirmed by the finding that the GF analog pairs that have the most bulky alkoxy substituent, showed the most prominent stereoselectivity for both AChE and BChE. The GA analog pairs are distinct from the other analog pairs because of the presence of the dimethylamino group instead of the methyl group. The steric difference between positioning the ethoxy group or the dimethylamino group in the acyl binding pocket is not significant. This is reflected by the < 4-fold stereoselectivity observed for GA model compounds reacting with both AChE and BChE. This low degree of stereoselectivity is in agreement with the reported ~7-fold difference in LD₅₀ for GA R_p and S_p isomers (41).

Stereoselectivities previously reported for inhibition of AChE and BChE by GD diastereomers was far greater than our results. DeBisschop *et al.* found a 300-fold difference between soman S_pS_c and R_pS_c for binding to human BChE (7). Ordentlich *et al.* reported a 40,000-fold difference between soman S_pS_c and R_pS_c for binding to human AChE (8). The results reported here for the GD model compounds might be less pronounced because of the presence of the racemic mixture about the carbon center of the pinacolyl group. While the configuration around the carbon atom of the pinacolyl group showed little selection on electric eel AChE, S_pR_c showed 2- and 10-fold lower potency than S_pS_c for human AChE (4,7,8). In addition, because the compounds were prepared as enantiomerically-enriched forms, we cannot rule out the

possibility of a small cross-contamination between the R_p and S_p isomers based on NMR analysis. A small percent cross contamination of the S_p isomer in the R_p preparation could limit the apparent inhibition rate for R_p to a small percent of that of the S_p isomer, thereby increasing the apparent potency for the R_p isomers. Because the **9** GF analog offered enough inhibition potency (k_i of $2.4 \times 10^6 \text{ M}^{-1}\text{min}^{-1}$), we were able to evaluate inhibition of **9- R_p** under sub-stoichiometric conditions (data not shown) and confirmed that the potential contamination of **9- S_p** should be less than 1%. Examining potential contamination R_p isomer in S_p isomer is technical challenging, however, the impact of a small percent cross-contamination from the R_p isomer on inhibition kinetics of the more reactive S_p isomer should be minor and off less concern. We conclude that the stereoselectivity determined from these enantiomerically-enriched compounds reported could represent an underestimated value of the true ratio from enantiomerically pure compounds. Regardless of this limitation, we believe these model compounds are useful tools for evaluation of stereoselectivity for different enzymes and for the application of the S_p isomers in the development of OP hydrolysis bioscavengers.

In summary, kinetic studies of the thiomethyl- and thiocholine-series of nerve agent model compounds revealed the potential as well as some limitations of these compounds for future applications. Simulation studies provide a molecular-level understanding of the orientation of the thiomethyl analogues prior to inhibition, and the docking modes obtained are consistent with the experimental findings. The stereoselectivity, enzyme selectivity, and dynamic range of inhibition potency of the two series of compounds suggest that the combined application of these model compounds will make them useful research tools for understanding interactions of nerve agents with cholinesterase and other enzymes of interest. These two series of compounds provide a useful panel of agents to examine the profile of enzyme interaction with GB, GF, GD, and GA. The distinct features contributed from the non-charged small thiomethyl group and the charged larger thiocholine group make them useful in studies comparing diverse OP compounds and enzyme interactions. The stereoselective inhibition of both AChE and BChE suggest that these model compounds (especially the thiocholine analogs) that produce the same phosphorylation enzyme adducts as the authentic nerve agents, can serve as useful tools to examine the stereoselectivity about the phosphorus chiral center for enzyme variants produced from bioscavenger development programs.

Acknowledgment

This research was supported by the National Institute of Health grant U54NS058183 Project 2 to JZ and Project 4 to CMH, U01NS058038 to JRC, and USAMRICD contract V91ZLK-06-R-0029 to JZ. We thank Dr. Oksana Lockridge and Dr. Lawrence Schopfer (UNMC, Omaha, NE), Dr. Florian Nachon (Centre de Recherches du Service de Santé des Armées, La Tronche, France), and Dr. Erik Ralph (Human BioMolecular Research Institute, San Diego, CA) for their critical discussions and valuable suggestions regarding the manuscript. We also thank Dr. Yongxuan Su (UCSD Molecular MS Facility, San Diego, CA) for MS and MS/MS analysis. Technical assistance of Ms. Melissa Ackley and Ms. Beilin Wang are also gratefully appreciated.

Abbreviations

OP, organophosphorus compounds
AChE, acetylcholinesterase
BChE, butyrylcholinesterase
ETP, echothiophate
GB, sarin
GD, soman
GF, cyclosarin
GA, tabun
VR, Russian VX
VX, (*S*-[2-(diisopropylamino)ethyl]-*O*-ethyl methylphosphonothioate)

ATCh, acetylthiocholine iodide
 BTCh, butyrylthiocholine iodide
 DTNB, 5,5'-dithiobis(2-nitrobenzoic acid)
 PTLT, preparative thin-layer chromatography
 TLC, thin-layer chromatography

References

1. Gunderson CH, Lehmann CR, Sidell FR, Jabbari B. Nerve Agents - A Review. *Neurology* 1992;42:946–950. [PubMed: 1315942]
2. Sussman JL, Harel M, Frolow F, Oefner C, Goldman A, Toker L, Silman I. Atomic-structure of acetylcholinesterase from *Torpedo-californica* - a prototypic acetylcholine-binding protein. *Science* 1991;253:872–879. [PubMed: 1678899]
3. Nachon F, Nicolet Y, Viguie N, Masson P, Fontecilla-Camps JC, Lockridge O. Engineering of a monomeric and low-glycosylated form of human butyrylcholinesterase: expression, purification, characterization and crystallization. *Eur J Biochem* 2002;269:630–637. [PubMed: 11856322]
4. Benschop HP, Konings CA, Van Genderen J, De Jong LP. Isolation, anticholinesterase properties, and acute toxicity in mice of the four stereoisomers of the nerve agent soman. *Toxicol Appl Pharmacol* 1984;72:61–74. [PubMed: 6710485]
5. Harvey SP, Kolakowski JE, Cheng T-C, Rastogi VK, Reiff LP, DeFrank JJ, Raushel FM, Hill C. Stereospecificity in the enzymatic hydrolysis of cyclosarin (GF). *Enzyme and Microbial Technology* 2005;37:547–555.
6. Ordentlich A, Barak D, Sod-Moriah G, Kaplan D, Mizrahi D, Segall Y, Kronman C, Karton Y, Lazar A, Marcus D, Velan B, Shafferman A. Stereoselectivity toward VX is determined by interactions with residues of the acyl pocket as well as of the peripheral anionic site of AChE. *Biochemistry* 2004;43:11255–11265. [PubMed: 15366935]
7. De Bisschop HC, Michiels KW, Vlamincx LB, Vansteenkiste SO, Schacht EH. Phosphorylation of purified human, canine and porcine cholinesterase by soman. Stereoselective aspects. *Biochem Pharmacol* 1991;41:955–959. [PubMed: 2009086]
8. Ordentlich A, Barak D, Kronman C, Benschop HP, De Jong LP, Ariel N, Barak R, Segall Y, Velan B, Shafferman A. Exploring the active center of human acetylcholinesterase with stereoisomers of an organophosphorus inhibitor with two chiral centers. *Biochemistry* 1999;38:3055–3066. [PubMed: 10074358]
9. Lenz DE, Yeung D, Smith JR, Sweeney RE, Lumley LA, Cerasoli DM. Stoichiometric and catalytic scavengers as protection against nerve agent toxicity: a mini review. *Toxicology* 2007;233:31–39. [PubMed: 17188793]
10. Masson P, Nachon F, Broomfield CA, Lenz DE, Verdier L, Schopfer LM, Lockridge O. A collaborative endeavor to design cholinesterase-based catalytic scavengers against toxic organophosphorus esters. *Chem Biol Interact* 2008;175:273–280. [PubMed: 18508040]
11. Millard CB, Lockridge O, Broomfield CA. Design and expression of organophosphorus acid anhydride hydrolase activity in human butyrylcholinesterase. *Biochemistry* 1995;34:15925–15933. [PubMed: 8519749]
12. Lockridge O, Blong RM, Masson P, Froment MT, Millard CB, Broomfield CA. A single amino acid substitution, Gly117His, confers phosphotriesterase (organophosphorus acid anhydride hydrolase) activity on human butyrylcholinesterase. *Biochemistry* 1997;36:786–795. [PubMed: 9020776]
13. Kovarik Z, Radic Z, Berman HA, Simeon-Rudolf V, Reiner E, Taylor P. Mutant cholinesterases possessing enhanced capacity for reactivation of their phosphorylated conjugates. *Biochemistry* 2004;43:3222–3229. [PubMed: 15023072]
14. Taylor P, Kovarik Z, Reiner E, Radic Z. Acetylcholinesterase: converting a vulnerable target to a template for antidotes and detection of inhibitor exposure. *Toxicology* 2007;233:70–78. [PubMed: 17196318]
15. Li WS, Lum KT, Chen-Goodspeed M, Sogorb MA, Raushel FM. Stereoselective detoxification of chiral sarin and soman analogues by phosphotriesterase. *Bioorg Med Chem* 2001;9:2083–2091. [PubMed: 11504644]

16. Amitai G, Adani R, Yacov G, Yishay S, Teitlboim S, Tveria L, Limanovich O, Kushnir M, Meshulam H. Asymmetric fluorogenic organophosphates for the development of active organophosphate hydrolases with reversed stereoselectivity. *Toxicology* 2007;233:187–198. [PubMed: 17129656]
17. Yeung DT, Smith JR, Sweeney RE, Lenz DE, Cerasoli DM. A gas chromatographic-mass spectrometric approach to examining stereoselective interaction of human plasma proteins with soman. *J Anal Toxicol* 2008;32:86–91. [PubMed: 18269799]
18. Berman HA, Leonard K. Chiral reactions of acetylcholinesterase probed with enantiomeric methylphosphonothioates. Noncovalent determinants of enzyme chirality. *J Biol Chem* 1989;264:3942–3950. [PubMed: 2917983]
19. Hosea NA, Berman HA, Taylor P. Specificity and orientation of trigonal carboxyl esters and tetrahedral alkylphosphonyl esters in cholinesterases. *Biochemistry* 1995;34:11528–11536. [PubMed: 7547883]
20. Hosea NA, Radic Z, Tsigelny I, Berman HA, Quinn DM, Taylor P. Aspartate 74 as a primary determinant in acetylcholinesterase governing specificity to cationic organophosphonates. *Biochemistry* 1996;35:10995–11004. [PubMed: 8718893]
21. Hall CR, Inch TD. Preparation and absolute-configuration of some chiral O,S-dialkyl phosphoramidothioates. *Tetrahedron Letters* 1977:3761–3764.
22. Hall CR, Inch TD. Chiral O,S-dialkyl phosphoramidothioates - their preparation, absolute-configuration, and stereochemistry of their reactions in acid and base. *Journal of the Chemical Society-Perkin Transactions* 1979;1:1646–1655.
23. Ellman GL, Courtney KD, Andres V Jr. Feather-Stone RM. A new and rapid colorimetric determination of acetylcholinesterase activity. *Biochem Pharmacol* 1961;7:88–95. [PubMed: 13726518]
24. Hart GJ, O'Brien RD. Recording spectrophotometric method for determination of dissociation and phosphorylation constants for the inhibition of acetylcholinesterase by organophosphates in the presence of substrate. *Biochemistry* 1973;12:2940–2945. [PubMed: 4737014]
25. Becke AD. Density-functional exchange-energy approximation with correct asymptotic behavior. *Phys Rev A* 1988;38:3098–3100. [PubMed: 9900728]
26. Becke AD. DENSITY-FUNCTIONAL THERMOCHEMISTRY .3. THE ROLE OF EXACT EXCHANGE. *Journal of Chemical Physics* 1993;98:5648–5652.
27. Lee CT, Yang WT, Parr RG. Development of the Colle-Salvetti correlation-energy formula into a functional of the electron-density. *Phys. Rev. B* 1988;37:785–789.
28. Frisch, MJ.; Trucks, GW.; Schlegel, HB.; Scuseria, GE.; Robb, MA.; Cheeseman, JR.; Montgomery, J.; J., A.; Vreven, T.; Kudin, KN.; Burant, JC.; Millam, JM.; Iyengar, SS.; Tomasi, J.; Barone, V.; Mennucci, B.; Cossi, M.; Scalmani, G.; Rega, N.; Petersson, GA.; Nakatsuji, H.; Hada, M.; Ehara, M.; Toyota, K.; Fukuda, R.; Hasegawa, J.; Ishida, M.; Nakajima, T.; Honda, Y.; Kitao, O.; Nakai, H.; Klene, M.; Li, X.; Knox, JE.; Hratchian, HP.; Cross, JB.; Bakken, V.; Adamo, C.; Jaramillo, J.; Gomperts, R.; Stratmann, RE.; Yazyev, O.; Austin, AJ.; Cammi, R.; Pomelli, C.; Ochterski, JW.; Ayala, PY.; Morokuma, K.; Voth, GA.; Salvador, P.; Dannenberg, JJ.; Zakrzewski, VG.; Dapprich, S.; Daniels, AD.; Strain, MC.; Farkas, O.; Malick, DK.; Rabuck, AD.; Raghavachari, K.; Foresman, JB.; Ortiz, JV.; Cui, Q.; Baboul, AG.; Clifford, S.; Cioslowski, J.; Stefanov, BB.; Liu, G.; Liashenko, A.; Piskorz, P.; Komaromi, I.; Martin, RL.; Fox, DJ.; Keith, T.; Al-Laham, MA.; Peng, CY.; Nanayakkara, A.; Challacombe, M.; Gill, PMW.; Johnson, B.; Chen, W.; Wong, MW.; Gonzalez, C.; Pople, JA. *Gaussian 03. Vol. Revision C.02 ed.*. Gaussian, Inc.; Wallingford CT: 2004.
29. Francel MM, Pietro WJ, Hehre WJ, Binkley JS, Gordon MS, Defrees DJ, Pople JA. Self-consistent molecular-orbital methods. 23. A polarization-type basis set for 2nd-row elements. *Journal of Chemical Physics* 1982;77:3654–3665.
30. Breneman CM, Wiberg KB. Determining atom-centered monopoles from molecular electrostatic potentials - the need for high sampling density in formamide conformational-analysis. *J. Comput. Chem* 1990;11:361–373.
31. Nicolet Y, Lockridge O, Masson P, Fontecilla-Camps JC, Nachon F. Crystal structure of human butyrylcholinesterase and of its complexes with substrate and products. *J Biol Chem* 2003;278:41141–41147. [PubMed: 12869558]

32. Morris GM, Goodsell DS, Halliday RS, Huey R, Hart WE, Belew RK, Olson AJ. Automated docking using a Lamarckian genetic algorithm and an empirical binding free energy function. *J. Comput. Chem* 1998;19:1639–1662.
33. Kryger G, Harel M, Giles K, Toker L, Velan B, Lazar A, Kronman C, Barak D, Ariel N, Shafferman A, Silman I, Sussman JL. Structures of recombinant native and E202Q mutant human acetylcholinesterase complexed with the snake-venom toxin fasciculin-II. *Acta Crystallogr D Biol Crystallogr* 2000;56:1385–1394. [PubMed: 11053835]
34. Marechal R, Bagot J. Muscarine-like action of some halogenated derivatives of alkyltrimethylammoniums (homologs of bromocholine). II. Chemistry. *Annales Pharmaceutiques Francaises* 1946;4:172–181.
35. Kovarik Z, Radic Z, Berman HA, Simeon-Rudolf V, Reiner E, Taylor P. Acetylcholinesterase active centre and gorge conformations analysed by combinatorial mutations and enantiomeric phosphonates. *Biochem J* 2003;373:33–40. [PubMed: 12665427]
36. Masson P, Froment MT, Bartels CF, Lockridge O. Importance of aspartate-70 in organophosphate inhibition, oxime re-activation and aging of human butyrylcholinesterase. *Biochem J* 1997;325(Pt 1):53–61. [PubMed: 9224629]
37. Krupka RM. Acetylcholinesterase: Trimethylammonium-Ion Inhibition of Deacetylation. *Biochemistry* 1964;3:1749–1754. [PubMed: 14235343]
38. Gilley C, MacDonald M, Nachon F, Schopfer LM, Zhang J, Cashman JR, Lockridge O. Nerve agent analogs that produce authentic soman, sarin, tabun, and cyclohexyl methylphosphonate-modified human butyrylcholinesterase. *Chem Res Toxicol*. 2009
39. Doorn, JA.; Schall, M.; Gage, DA.; Talley, TT.; Thompson, CM.; Richardson, RJ. Identification of butyrylcholinesterase adducts after inhibition with isomalathion using mass spectrometry: Difference in mechanism between (1R)- and (1S)-stereoisomers. 2001. p. 73-80.
40. Doorn JA, Talley TT, Thompson CM, Richardson RJ. Probing the active sites of butyrylcholinesterase and cholesterol esterase with isomalathion: conserved stereoselective inactivation of serine hydrolases structurally related to acetylcholinesterase. *Chem Res Toxicol* 2001;14:807–813. [PubMed: 11453726]
41. Degenhardt C, Vandenberg GR, Dejong LPA, Benschop HP, Vangenderen J, Vandemeent D. Enantiospecific complexation gas-chromatography of nerve agents - isolation and properties of the enantiomers of ethyl N,N-dimethylphosphoramidocyanidate (tabun). *Journal of the American Chemical Society* 1986;108:8290–8291.

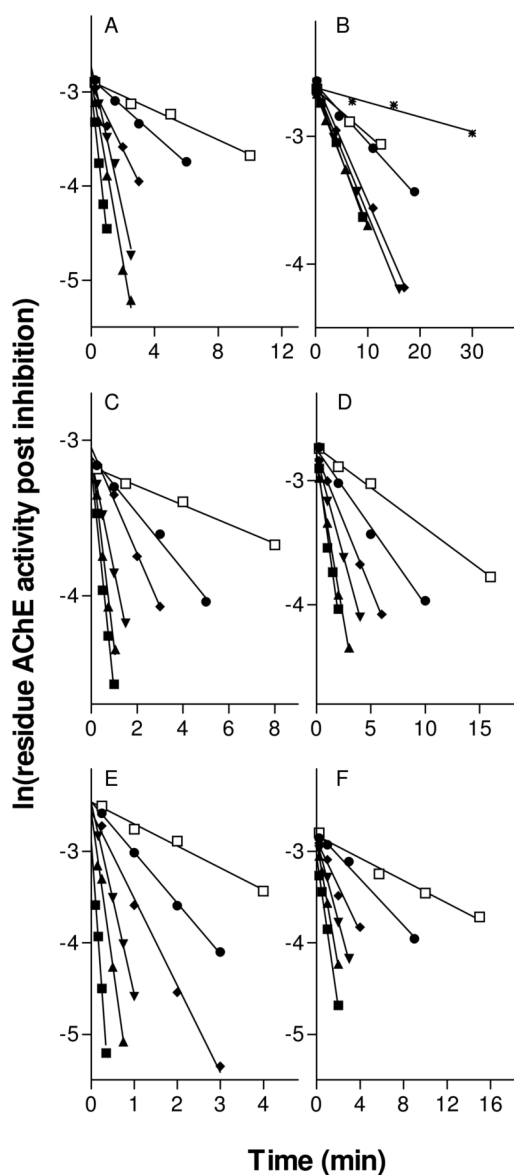


Figure 1.

Representative time course studies of human AChE inhibition by the thiomethyl analogs: (A) 5-S_p, (B) 5-R_p, (C) 6-S_p, (D) 6-R_p, (E) 7-S_p, and (F) 7-R_p. Human AChE was incubated with a diverse range concentration of analogs for the indicated period of time. The residue activity post inhibition was determined by the Ellman assay. Natural log of the activity was plotted as a function of the duration of enzyme inhibition with inhibitors and fitted to a linear regression curve. Best fitted slope values define the apparent rate constants k_{app} .

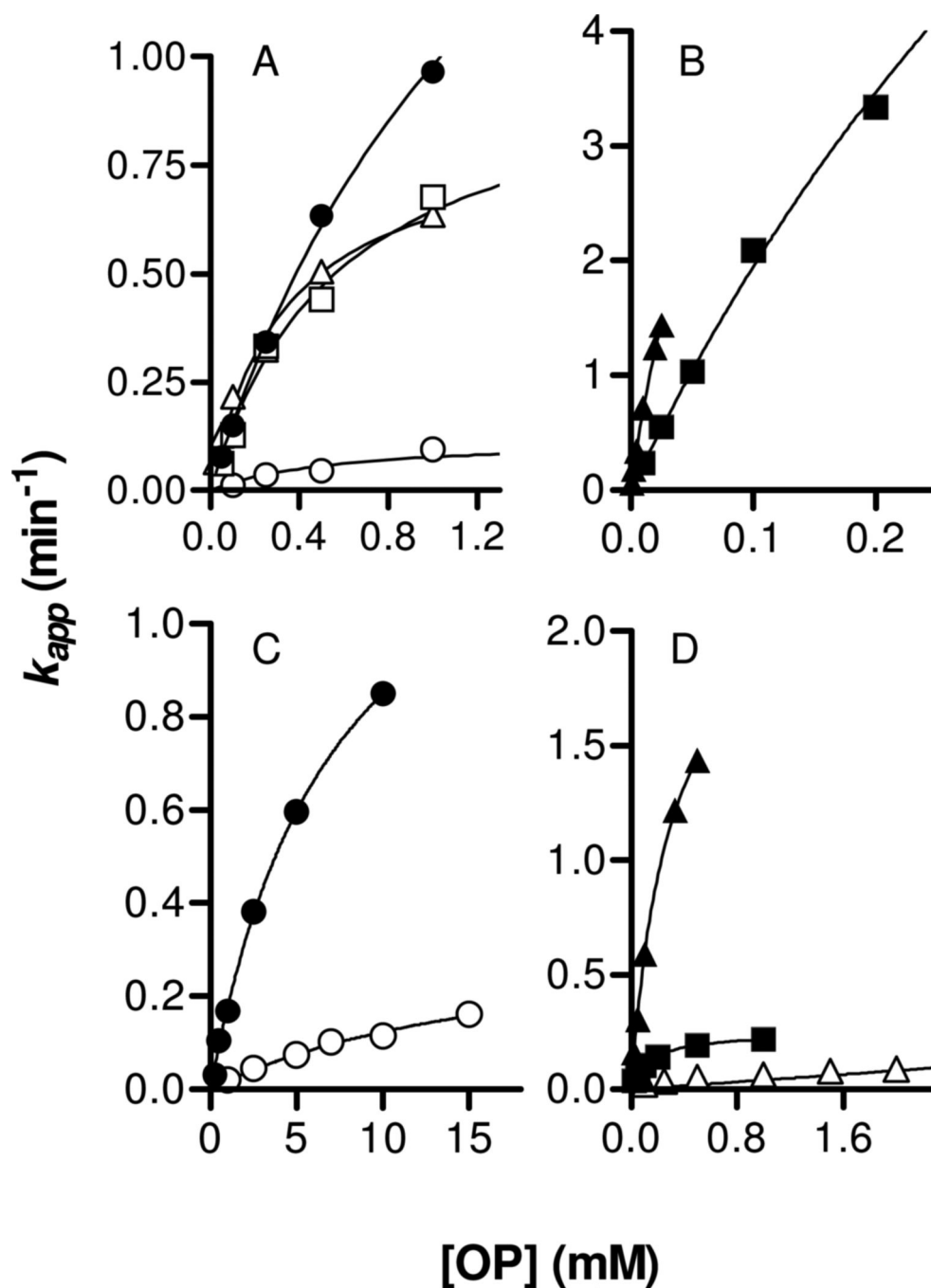


Figure 2.

Re-plot of k_{app} versus inhibitor concentration for the incubations of AChE (A, B) and BChE (C, D) with the thiomethyl analogs: **5-*S_p*** (filled circle), **5-*R_p*** (open circle), **6-*S_p*** (filled triangle), **6-*R_p*** (open triangle), **7-*S_p*** (filled square), and **7-*R_p*** (open square). The best-fitted k_{app} values were derived from slopes of linear regression analysis as shown in Figure 1. Data were fitted to the equation of $k_{app} = k_2[OP]/(K_D + [OP])$.

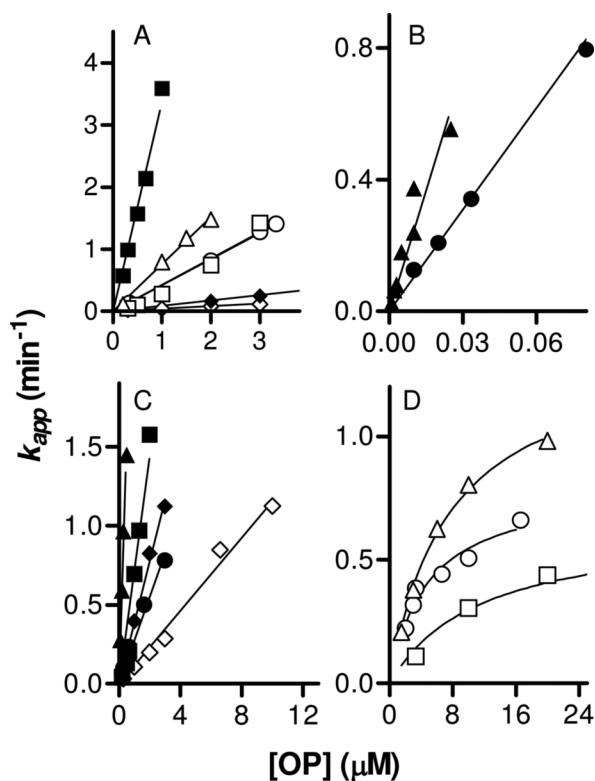


Figure 3.

Re-plot of k_{app} versus inhibitor concentration for the reactions of AChE (A, B) and BChE (C, D) with the thiocholine analogs: **8- S_p** (filled circle), **8- R_p** (open circle), **9- S_p** (filled triangle), **9- R_p** (open triangle), **10- S_p** (filled square), **10- R_p** (open square), **11- S_p** (filled diamond), and **11- R_p** (open diamond). The points indicate the best-fitted k_{app} values (data not shown). Data was fitted to a linear curve in 3A, 3B, and 3C. Data was fitted to the equation of $k_{app} = k_2[OP]/(K_D + [OP])$ in 3D.

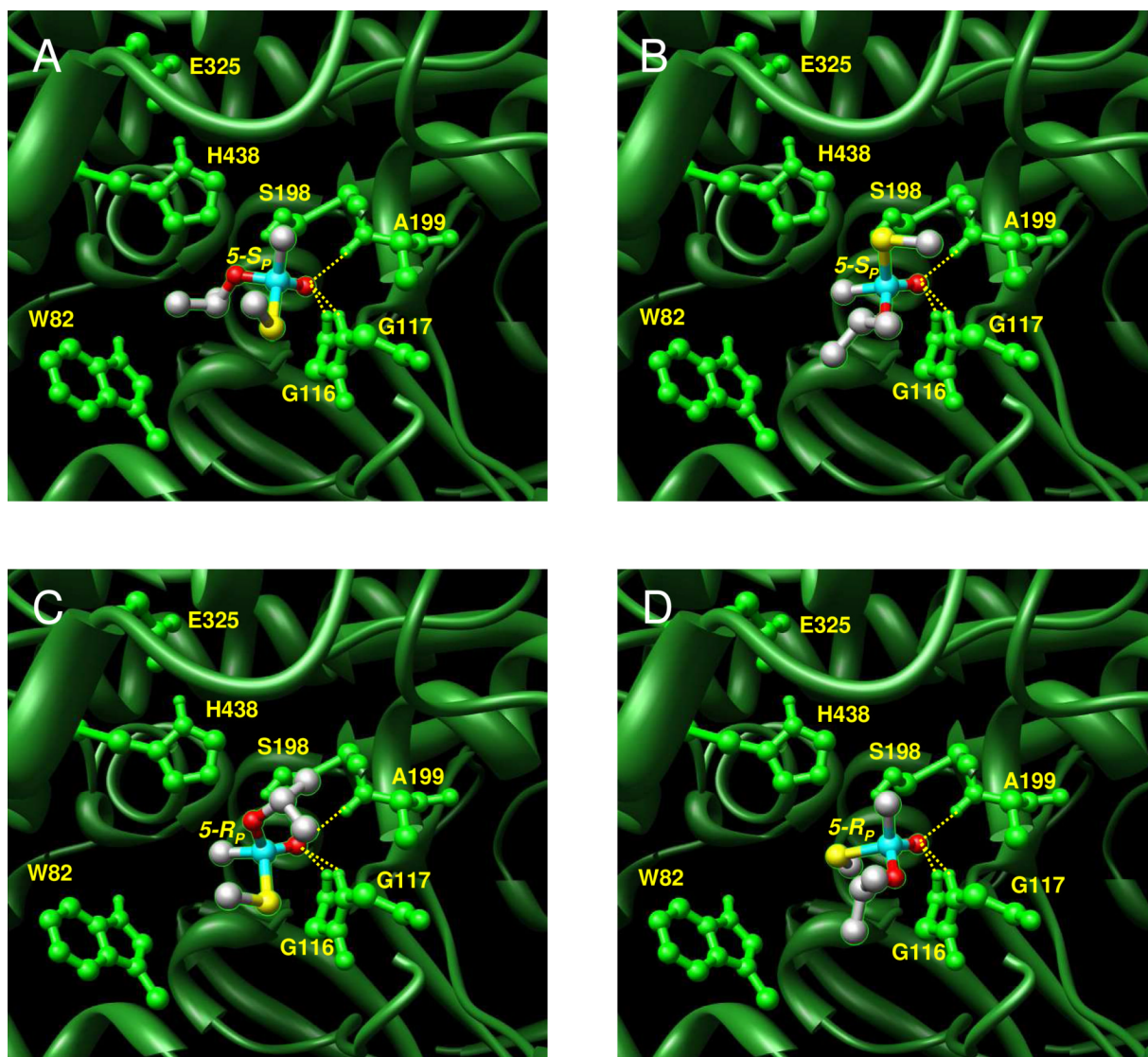
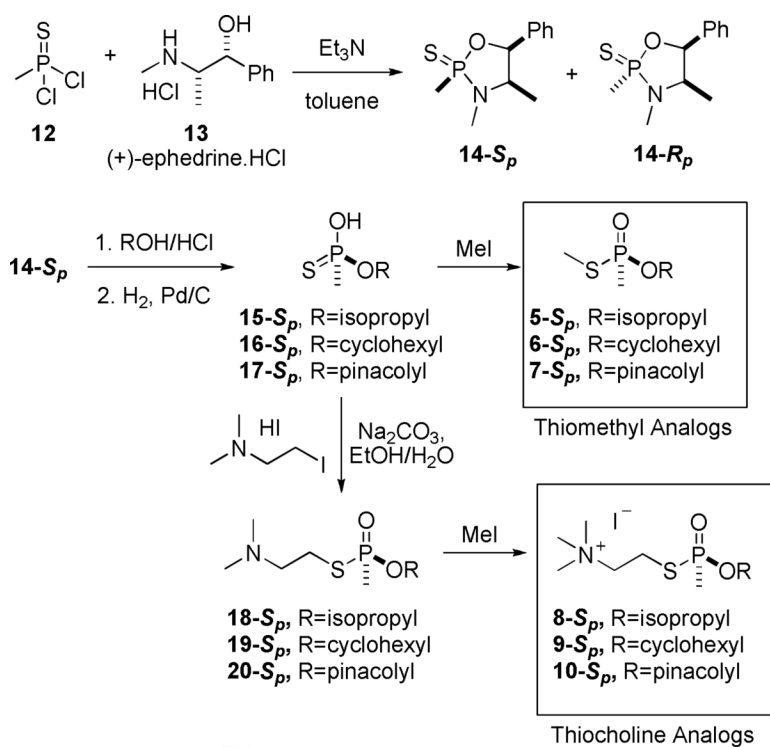
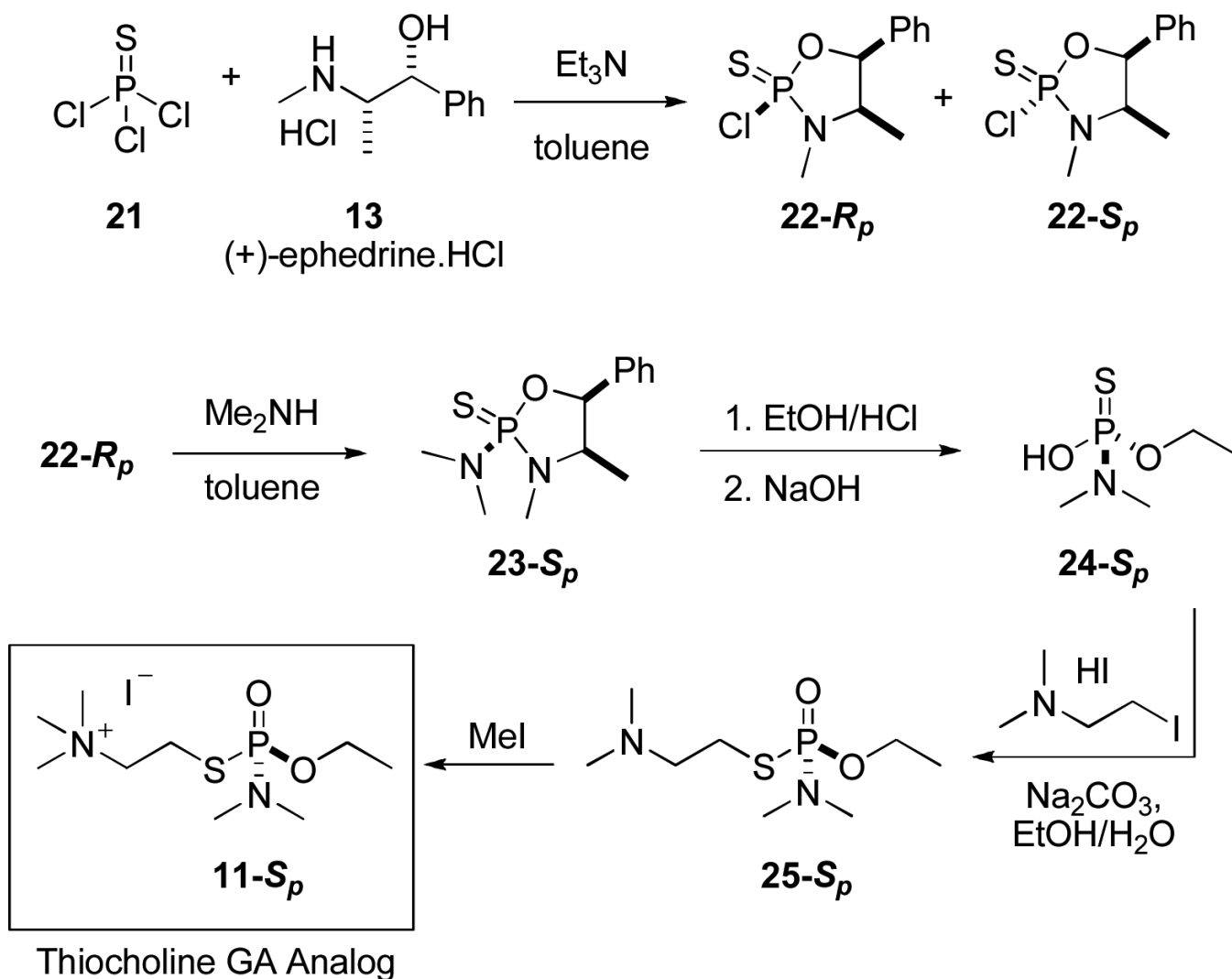


Figure 4.

Preferred docking positions for (A) $5-S_p$ ($-SMe$ as the leaving group), (B) $5-S_p$ ($-OR$ as the leaving group), (C) $5-R_p$ ($-SMe$ as the leaving group), and (D) $5-R_p$ ($-OR$ as the leaving group) in the catalytic gorge of human BChE (PDB ID: 1P0I). The energy for each preferred orientation was -6.18 (A), -6.42 (B), -6.02 (C), and -6.26 (D) kcal mol^{-1} , respectively.

**Scheme 1.**

Chemical synthesis of enantiomerically enriched S_p nerve agent model compounds for GB, GF, and GD (5-S_p to 10-S_p). Diastereomers 14-S_p and 14-R_p obtained from the first step of synthesis were separated as described in the text. The synthesis of R_p nerve agent model compounds followed the same scheme using intermediate 14-R_p (scheme not shown).

**Scheme 2.**

Chemical synthesis of enantiomerically enriched S_p nerve agent model compounds for GA (**11- S_p**). Diastereomers **22- S_p** and **22- R_p** obtained from the first step of synthesis were separated as described in the text. The synthesis of R_p nerve agent model compounds followed the same scheme using intermediate **22- S_p** (scheme not shown).

Table 1

Chemical structures for nerve agents model compounds corresponding to thiomethyl analogs and thiocholine analogs.

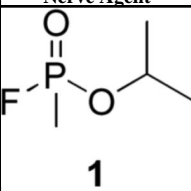
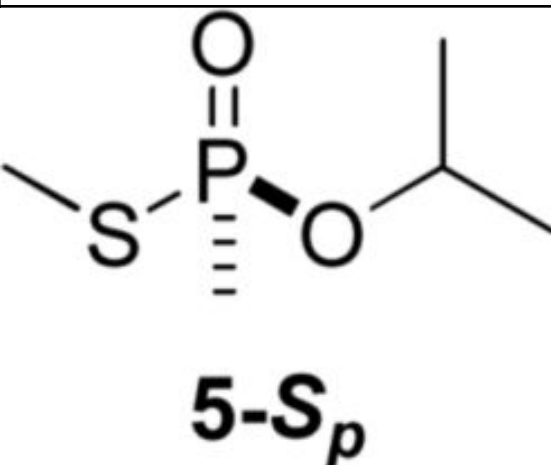
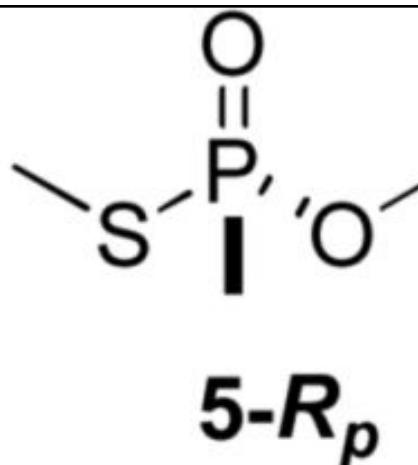
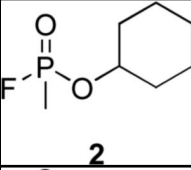
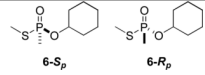
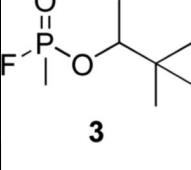
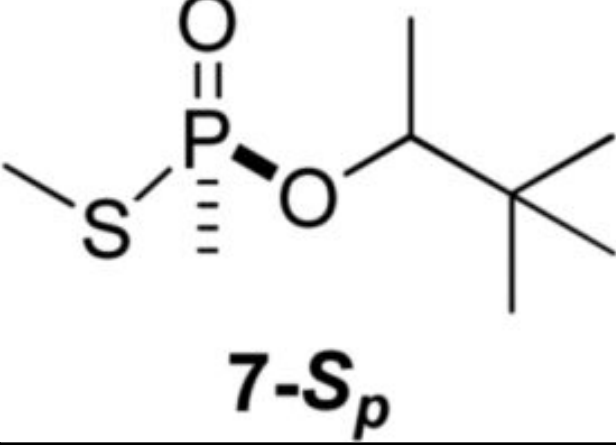
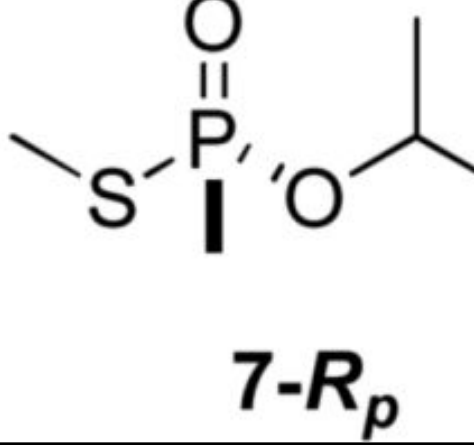
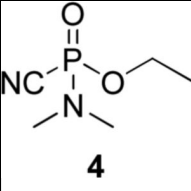
	Nerve Agent	Thiomethyl Analogs
sarin (GB)	 <p>1</p>	 <p>5-S_p</p>  <p>5-R_p</p>
cyclosarin (GF)	 <p>2</p>	 <p>6-S_p 6-R_p</p>
soman (GD)	 <p>3</p>	 <p>7-S_p</p>  <p>7-R_p</p>
tabun (GA)	 <p>4</p>	

Table 2
Kinetic parameters for inhibition of AChE and BChE by thiomethyl nerve agent model compounds.

Thiomethyl analogs	AChE			BChE		
	k_i^a (mM ⁻¹ min ⁻¹)	k_2^b (min ⁻¹)	K_D^c (mM)	k_i^a (mM ⁻¹ min ⁻¹)	k_2^b (min ⁻¹)	K_D^c (mM)
GB <i>5-S_p</i> <i>5-R_p</i> <i>S_p/R_p ratio</i>	1.6 ± 0.08	2.4 ± 0.06	1.50 ± 0.07	0.2 ± 0.02	1.47 ± 0.06	7.3 ± 0.6
	0.17 ± 0.03	0.12 ± 0.01	0.72 ± 0.11	0.018 ± 0.01	0.24 ± 0.04	10.9 ± 2.7
	9.4			11		
GF <i>6-S_p</i> <i>6-R_p</i> <i>S_p/R_p ratio</i>	79.6 ± 19.05	5.34 ± 0.8	0.07 ± 0.01	10.3 ± 1.7	1.5 ± 0.07	0.14 ± 0.02
	2.86 ± 0.18	0.81 ± 0.01	0.28 ± 0.02	0.22 ± 0.04	0.10 ± 0.01	0.45 ± 0.08
	28			47		
GD <i>7-S_p</i> <i>7-R_p</i> <i>S_p/R_p ratio</i>	22.1 ± 3.22	16 ± 1.3	0.72 ± 0.09	1.7 ± 0.07	0.25 ± 0.01	0.15 ± 0.01
	1.7 ± 0.26	1.02 ± 0.05	0.59 ± 0.08	—	—	—
	13			—		

^a Bimolecular inhibition constant (k_i)

^b Phosphorylation constant (k_2)

^c Equilibrium dissociation constant (K_D) All values for k_2 , and K_D were derived from non-linear curve fit of k_{app} over analog concentrations. Values reported represent best fit values ± standard error derived from fitting 30–40 data points from a single experiment. All values for k_i were calculated from ratios of k_2/K_D . Stereoselectivities were defined by the S_p/R_p ratio of k_i values.

Table 3
Kinetic parameters for inhibition of AChE and BChE by thiocholine nerve agent model compounds.

Thiocholine analogs	AChE		BChE	
	k_i^a ($\mu\text{M}^{-1}\text{min}^{-1}$)	k_i^a ($\mu\text{M}^{-1}\text{min}^{-1}$)	k_2^b (min^{-1})	K_D^c (μM)
GB	$8\text{-}S_p$	10.2 ± 0.3	—	—
	$8\text{-}R_p$	0.43 ± 0.01	0.85 ± 0.07	5.8 ± 1.2
	S_p/R_p ratio	24 2.5		
GF	$9\text{-}S_p$	38.9 ± 1.7	—	—
	$9\text{-}R_p$	0.75 ± 0.04	0.66 ± 0.03	4.2 ± 0.4
	S_p/R_p ratio	52 16		
GD	$10\text{-}S_p$	3.7 ± 0.2	—	—
	$10\text{-}R_p$	0.50 ± 0.04	0.57 ± 0.03	11.0 ± 2.4
	S_p/R_p ratio	7.3 19		
GA	$11\text{-}S_p$	0.093 ± 0.003	—	—
	$11\text{-}R_p$	0.035 ± 0.003	—	—
	S_p/R_p ratio	2.5 3.6		
ETP		1.8 ± 0.09	—	—

When k_2 and K_D are not reported, values for k_i were derived from the slope of linear curve fit of k_{app} over analog concentrations. Values reported represent best fit values \pm standard error derived from fitting 30-40 data points from a single experiment.

Stereoselectivities were defined by the S_p/R_p ratio of k_i values.

^aBimolecular inhibition constant (k_i)

^bPhosphorylation constant (k_2)

^cEquilibrium dissociation constant (K_D) When k_2 and K_D are reported, all values were derived from non-linear curve fit of k_{app} over analog concentrations. Values reported represent best fit values \pm standard error. Values for k_i were calculated from ratios of k_2/K_D .